Vietnam Journal of Mechanics, Vietnam Academy of Science and Technology
DOI: https://doi.org/10.15625/0866-7136/23885

STRESS ANALYSIS OF ANISOTROPIC HYBRID COMPOSITE PLATES WITH LOADED HOLES

Nguyen Cong Minh, Nguyen Hoang Quan, Nguyen Van Thuong*
School of Aerospace Engineering, VNU University of Engineering and Technology, Hanoi, Vietnam
E-mail: thuong.nv@vnu.edu.vn

Received: 5 December 2025 / Revised: 30 December 2025 / Accepted: 31 December 2025
Published online: 3 April 2026

Abstract. In this paper, a stress analysis of hybrid anisotropic composite plates with loaded holes is performed using the boundary-based finite element method (BFEM). Here, the hybrid composite plates may consist of different anisotropic elastic materials. To apply the BFEM, we divide the plate into different regions, each of which is made of different anisotropic elastic constants. The BFEM combines the boundary elements in each region into a single finite element and assembles them following the rules of the finite element method. This method, therefore, does not require volumetric meshing, which is beneficial for meshing and computational costs. The BFEM can be applied to general anisotropic hybrid elastic plates and various loaded hole situations, e.g., pressurized holes or prescribed displacements on the holes. With the BFEM, numerical examples are performed. The numerical results will be used for verification and parametric study purposes. In the verification, we compare the results obtained by the BFEM with those obtained by other available solution methods. The parametric studies investigate the effects of the anisotropic material properties and applied pressurized loads/displacements on the stress distribution around the hole.

Keywords: anisotropic hybrid composite, loaded hole, boundary-based finite element method, pressurized hole, interference fit.

1. INTRODUCTION

Hybrid composites are now widely used in many engineering applications, such as in aircraft structures and biomedical applications (Jamir et al., 2018; Puttegowda et al., 2018; Wintermantel et al., 2001). These materials are often constructed from two or more different types of materials or different types of fibers within a common matrix (Jamir et al., 2018; Puttegowda et al., 2018; Wintermantel et al., 2001). Rivet/bolt/pin joints are usually adopted in the assembly of structural components in these engineering applications due to their low cost and ease of assembly and disassembly (Abazadeh & Shishevan, 2019; Bahloul et al., 2018; Bi et al., 2015; Wang et al., 2023; Zhang & Zhou, 2022; Zuo et al., 2020). When the hole is subjected to rivet/bolt/pin joints, it may experience either radial compressions or pre-stresses, causing it to expand (Li et al., 2015; H. Q. Nguyen et al., 2025). Many published works have shown that by properly controlling the radial compressions or pre-stresses around the loaded hole, the distribution of the stress around the hole can be controlled, which then enhances the performance and lifetime of the structure (Song et al., 2016; Xu et al., 2020). Understanding the behavior of a hybrid composite plate with loaded holes, therefore, is crucial in many engineering applications.

In the literature, many researchers have made great efforts to solve the problems of loaded holes within anisotropic composite plates (Chen & Hwu, 2014; Hwu, 2021; Lie et al., 2000;

V. T. Nguyen et al., 2025; Nguyen-Hoang & Becker, 2022; Pham & Weijermars, 2020; Rust, 2015; Toubal et al., 2005; Weijermars et al., 2020; Wu & Mu, 2003). In these published papers, different methods are used, such as the analytical solution method (Pham & Weijermars, 2020; Weijermars et al., 2020), boundary element method (Chen & Hwu, 2014; Lie et al., 2000), and finite element method (Rust, 2015). Among the different methods, analytical solutions are applied only to problems with simple boundary conditions for an infinite plate due to their inherent limitations. The finite element methods and boundary element methods are applied to more complicated problems with actual geometries and boundary conditions. When applying to problems with holes/cracks, especially multiple holes/cracks, the finite element method reveals a shortcoming, i.e., very fine meshes are required in the vicinity of the holes and cracks. This limitation leads to extensive computational time and a high demand for resources. The boundary element method has been proven to be a powerful tool in handling problems with holes and/or cracks (V. T. Nguyen & Hwu, 2017, 2018). This method, however, can only be applied to problems of homogeneous composite plates. When considering anisotropic hybrid composite materials, the boundary-based finite element method (Hwu et al., 2017) can be used. In this method, we can divide the anisotropic hybrid composite plate into N subregions. Each subregion is made of a different material, and then we can apply boundary elements to it. With the boundary elements for each subregion, by using the relation between the surface traction in BEM and the nodal force in the finite element method, a boundary-based finite element (BFEM) formulation for the whole anisotropic hybrid composite plate can be established. Using BFEM in solving problems with loaded holes in an anisotropic hybrid composite plate possesses several advantages, such as the formulation remains in the boundary-discretization only, and as a result, the meshing and computational efforts and resources can be reduced.

From the above-mentioned motivations, in this paper, the boundary-based finite element method is employed to solve problems of loaded holes in anisotropic hybrid composite plates. To demonstrate the correctness and applicability of the method, several numerical examples are provided. They include two circular holes in a homogeneous anisotropic composite plate, two circular holes in an anisotropic hybrid composite plate, and an interference fit assembly in an anisotropic hybrid composite plate. In these examples, the numerical results of the BFEM are compared with the conventional BEM for a homogeneous anisotropic composite plate. Based on the results, parametric studies are performed to investigate the effects of interference fits and material anisotropy on the stress distribution around the holes. This information will provide useful guidance in design and enhance the performance of such structures in engineering applications.

2. PROBLEM DESCRIPTIONS

We consider the problems of an anisotropic hybrid composite plate containing N subregions, where each subregion is made of a different anisotropic elastic material, which may be caused by its own fiber orientation, denoted by the angle β_k, $k = 1, 2, \ldots, N$ (Fig. 1). In each subregion, the basic equations for the anisotropic composite materials can be described by

$$\sigma_{ij}^{(k)} = C_{ijpq}^{(k)} \varepsilon_{pq}^{(k)}, \quad \varepsilon_{pq}^{(k)} = \frac{1}{2}\left(u_{p,q}^{(k)} + u_{q,p}^{(k)}\right), \quad \sigma_{ij,j}^{(k)} = 0, \quad i, j, p, q = 1, 2, 3, \tag{1}$$

where k denotes the k^{th} subregion; $u_{p,q}^{(k)}$, $\varepsilon_{pq}^{(k)}$ and $\sigma_{ij}^{(k)}$ represent the displacement, strain, and stress components of this subregion, respectively; $C_{ijpq}^{(k)}$ is the fourth-order stiffness tensor describing the elastic behavior of an anisotropic material with up to 21 independent constants. The comma stands for differentiation, and the repeated index means the summation of the related parameter over this index.

The analysis is conducted in a two-dimensional domain under the plane stress assumption, which is appropriate for thin composite plates subjected to in-plane loading. By dividing the

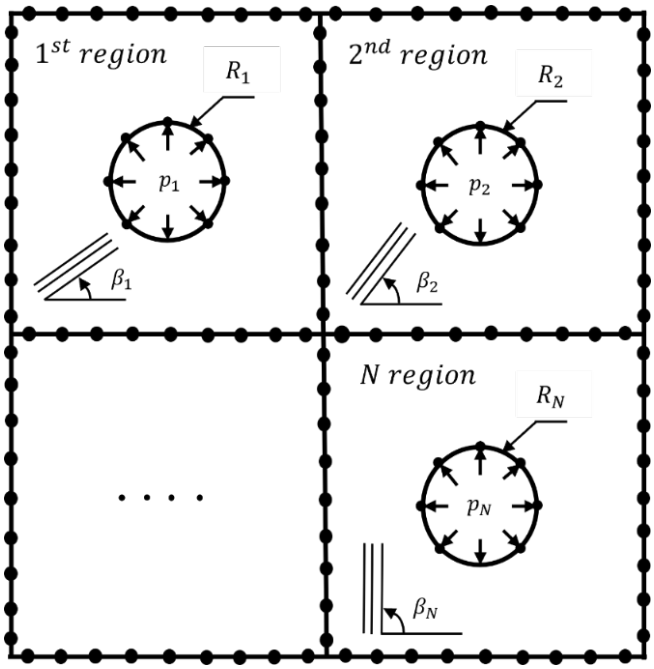

Fig. 1. An anisotropic hybrid plate with N loaded holes

anisotropic hybrid composite into N subdomains, we can apply the conventional BEM to each domain. In the BEM, the boundary element formulation is constructed using the fundamental solution for an infinite anisotropic elastic composite plate (Chen & Hwu, 2014; Hwu, 2021). With this fundamental solution, the BEM can accurately capture the directional dependence behaviors (anisotropic behaviors) in each region , with only boundary elements and nodes needed in each subregion. The boundary element integral equations for each subregion can be written as (Hwu, 2021)

$$\begin{aligned} c_{ij}^{(k)}(\boldsymbol{\xi}^{(k)})u_j^{(k)}(\boldsymbol{\xi}^{(k)}) + \int_{\Gamma_k} t_{ij}^{*(k)}(\mathbf{x}^{(k)},\boldsymbol{\xi}^{(k)})u_j^{(k)}(\mathbf{x}^{(k)})\,\mathrm{d}\Gamma_k(\mathbf{x}^{(k)}) \\ = \int_{\Gamma_k} u_{ij}^{*(k)}(\mathbf{x}^{(k)},\boldsymbol{\xi}^{(k)})t_j^{(k)}(\mathbf{x}^{(k)})\,\mathrm{d}\Gamma_k(\mathbf{x}^{(k)}), \quad i,j=1,2,3, \end{aligned} \tag{2}$$

where Γ_k is the boundary of the k^{th} subregion; $u_j^{(k)}(\mathbf{x}^{(k)})$ and $t_j^{(k)}(\mathbf{x}^{(k)})$ are the displacements and tractions at the field point $\mathbf{x}^{(k)}$ on the boundary Γ_k; $t_{ij}^{*(k)}$ and $u_{ij}^{*(k)}$ are the fundamental solutions of traction and displacement; $c_{ij}^{(k)}(\boldsymbol{\xi}^{(k)})$ is the coefficient, whose determination depends on the location of the source point $\boldsymbol{\xi}^{(k)}$, i.e., we have $c_{ij}^{(k)}(\boldsymbol{\xi}^{(k)}) = \delta_{ij}/2$ if $\boldsymbol{\xi}^{(k)}$ is located on a smooth boundary and $c_{ij}^{(k)}(\boldsymbol{\xi}^{(k)}) = \delta_{ij}$ if $\boldsymbol{\xi}^{(k)}$ is located inside the subregion in which δ_{ij} is Kronecker delta. By dividing the boundary Γ_k into m elements and S nodes, following the standard procedure of the BEM, we can obtain the following systems of algebraic equations (Hwu, 2021)

$$\sum_{s=1}^{S} \mathbf{Y}_{is}^{(k)}\mathbf{u}_s^{(k)} = \sum_{s=1}^{S} \mathbf{G}_{is}^{(k)}\mathbf{t}_s^{(k)}, \quad i=1,2,\ldots,S, \tag{3}$$

where $\mathbf{u}_s^{(k)}$ and $\mathbf{t}_s^{(k)}$ are the displacement and traction vectors at node s on the boundary Γ_k; $\mathbf{Y}_{is}^{(k)}$ and $\mathbf{G}_{is}^{(k)}$ are the influence matrices associated with nodes i and s, and their determination depends on the choices of the interpolation functions and fundamental solutions. In this study, the quadratic shape function is selected for the interpolation, and the fundamental solutions are

selected as the fundamental solution for an infinite anisotropic elastic plate (Hwu, 2021), i.e.,

$$\begin{aligned}[u_{ij}^{*(k)}] &= 2\,\mathrm{Re}[\mathbf{A}^{(k)}\mathbf{F}^{(k)}(z^{(k)})]^T,\\ [t_{ij}^{*(k)}] &= 2\,\mathrm{Re}[\mathbf{B}^{(k)}\mathbf{F}_{,s}^{(k)}(z^{(k)})]^T,\end{aligned} \tag{4}$$

where Re denotes the real part of a complex number; $\mathbf{A}^{(k)}$ and $\mathbf{B}^{(k)}$ are the matrices of material eigenvectors, obtained by using the elastic stiffness tensor $C_{ijpq}^{(k)}$ for each subregion. $\mathbf{F}^{(k)}(z^{(k)})$ is the holomorphic complex function vector, which is defined as follows for problems of an anisotropic elastic plate

$$\begin{aligned}&\mathbf{F}^{(k)}(z^{(k)}) = \frac{1}{2\pi i}\langle \ln(z_\alpha^{(k)} - \hat{z}_\alpha^{(k)})\rangle [\mathbf{A}^{(k)}]^T,\\ &z_\alpha^{(k)} = x_1^{(k)} + \mu_\alpha^{(k)} x_2^{(k)}, \quad \hat{z}_\alpha^{(k)} = \hat{x}_1^{(k)} + \mu_\alpha^{(k)}\hat{x}_2^{(k)}, \quad \alpha = 1,2,3,\end{aligned} \tag{5}$$

and $\mathbf{x} = (x_1^{(k)}, x_2^{(k)})$, $\boldsymbol{\xi} = (\hat{x}_1^{(k)}, \hat{x}_2^{(k)})$ are the locations of field point and source point; the symbol $\langle\rangle$ denotes a diagonal matrix whose components vary according to subscript α; $\mu_\alpha^{(k)}$ is the material eigenvalue associated with the eigenmatrices $\mathbf{A}^{(k)}$ and $\mathbf{B}^{(k)}$; $\mathbf{F}_{,s}^{(k)}(z^{(k)}) = \partial\mathbf{F}^{(k)}(z^{(k)})/\partial s$ where s is the tangential direction on the boundary. For the detailed evaluations of $\mathbf{Y}_{is}^{(k)}$ and $\mathbf{G}_{is}^{(k)}$, readers may refer to Section 15.4 in Hwu (2021).

If we treat the subregion enclosed by the boundary element as a super finite element, the systems of linear equations in BEM can be written as

$$\mathbf{Y}_e^{(k)}\mathbf{u}_e^{(k)} = \mathbf{G}_e^{(k)}\mathbf{t}_e^{(k)}, \tag{6}$$

where $\mathbf{u}_e^{(k)}$ and $\mathbf{t}_e^{(k)}$ are, respectively, the vectors for the nodal displacements and tractions of all nodes in each subregion. $\mathbf{Y}_e^{(k)}$ and $\mathbf{G}_e^{(k)}$ are the global influence matrices for each subregion, obtained by assembling their constituent influence matrices $\mathbf{Y}_{is}^{(k)}$ and $\mathbf{G}_{is}^{(k)}$ as mentioned in Eq. (3) (Hwu, 2021).

By using the relation between the surface traction $\mathbf{t}_e^{(k)}$ of the boundary elements in BEM and the nodal force $\mathbf{f}_e^{(k)}$ of the finite element in FEM, we can convert the system of linear equations (6) into (Hwu, 2021)

$$\mathbf{K}_e^{(k)}\mathbf{u}_e^{(k)} = \mathbf{f}_e^{(k)}, \tag{7}$$

where

$$\mathbf{f}_e^{(k)} = \sum_{m=1}^{M}\int_{\Gamma_m}\mathbf{N}^T\left(\mathbf{N}\mathbf{t}_m^{(k)}\right)\mathrm{d}\Gamma_m = \sum_{m=1}^{M}\mathbf{W}_m^{(k)}\mathbf{t}_m^{(k)} = \mathbf{W}_e^{(k)}\mathbf{t}_e^{(k)}, \tag{8}$$

and

$$\mathbf{K}_e^{(k)} = \mathbf{W}_e^{(k)}\left[\mathbf{G}_e^{(k)}\right]^{-1}\mathbf{Y}_e^{(k)}. \tag{9}$$

In the above equation, $\mathbf{N}$ is the set of shape functions, $\mathbf{t}_m^{(k)}$ is the traction of the m^{th} boundary element in the k^{th} subregion, and $\mathbf{K}_e^{(k)}$ is the element stiffness matrix in FEM. It should be noted that to compute the stiffness matrix from Eq. (9), the inversion of $\mathbf{G}_e^{(k)}$ is required. To prevent the potential singularity of $\mathbf{G}_e^{(k)}$, the double nodes commonly used at boundary element corners should be modeled as two distinct nodes with slightly offset positions rather than coincident locations (Hwu, 2021).

With the finite element formulation in Eq. (7) for each subregion, by assembling all subregions together following the rules of FEM, we can obtain the final system of linear equations in the BFEM. By solving the system of linear equations in the BFEM, the displacement solution can be obtained. It should be mentioned that with the transformations in Eqs. (7)–(9), no volumetric

meshing is required in the BFEM. Only the boundary discretization is needed. This method is beneficial in terms of reducing meshing effort and computational resources, which can serve as a powerful tool for solving problems of anisotropic hybrid composite plates with loaded holes.

3. NUMERICAL EXAMPLES

In this section, several numerical examples are provided to demonstrate the correctness and applicability of the BFEM in solving problems involving anisotropic hybrid composite plates with loaded holes. They include (1) a homogeneous composite plate with two loaded holes, (2) an anisotropic hybrid composite plate with two loaded holes, and (3) interference fits in an anisotropic hybrid composite plate. All computations were performed using MATLAB on a computer equipped with an Intel Core i7 processor and 16 GB of RAM.

3.1. A homogeneous composite plate with two loaded holes

Consider two loaded holes in a homogeneous composite plate, as shown in Fig. 2. The holes have circular shapes of the same radius $R_1 = R_2 = R = 5$ mm and are located at a distance of $d/R = 5$. They are loaded by uniform internal pressures $p_1 = p_2 = \sigma = 50$ MPa. The plate has the dimensions of $W = L = 1$ m and is made of a unidirectional fiber composite whose material properties are

$$E_{11} = 134, \quad E_{22} = E_{33} = 11, \quad G_{12} = G_{34} = 5.84, \quad G_{23} = 2.89, \quad \nu_{12} = \nu_{13} = 0.3, \quad \nu_{23} = 0.49, \tag{10}$$

where E and G denote the elastic and shear moduli of the material (GPa); ν denotes the Poisson ratio of the material; the subscripts 1 and 2 denote the fiber and transverse directions, and 3 denotes the direction normal to the plate.

Table 1. Mesh convergence study: hoop stress at selected points on the right hole boundary

θ	72 points	180 points	360 points	Diff. (%) (72→360)	Diff. (%) (180→360)
90°	1.4751	1.4757	1.4801	0.34	0.30
180°	1.4475	1.4480	1.4475	0.00	0.03

Table 2. Hoop stress on the right hole

θ	BFEM	BEM	Diff. (%)
90°	1.4757	1.4764	0.05
180°	1.4480	1.4483	0.03
270°	1.4757	1.4764	0.05

To solve the problem using the BFEM, the plate is divided into two subregions, as illustrated in Fig. 2. Each subregion is discretized into boundary elements and nodes. To ensure the reliability of the numerical results, a mesh convergence study is conducted. Table 1 presents the convergence behavior of the hoop stress at selected locations along the right hole boundary obtained using three different boundary discretizations with 72, 180, and 360 nodes uniformly distributed along each circular hole. The number of nodes on the outer boundaries and the shared interface between the two subregions is kept unchanged. As the boundary mesh is refined, the computed hoop stress values show only minor variations and gradually stabilize. The maximum relative difference between the coarsest discretization (72 points) and the finest discretization (360 points) is less than 0.35%, whereas the difference between the intermediate

discretization (180 points) and the finest one is less than 0.30%. Based on this observation, a boundary discretization with 180 points per hole was adopted.

With this choice of hole discretization, a total of 727 nodes and 460 elements were employed in the BFEM, including those on the outer boundaries, the two holes, and the shared interface between the two subregions. This resulted in a computation time of 114.1 s. In contrast, the conventional BEM requires only 524 nodes and 260 elements on the outer boundaries and holes, leading to a shorter computation time of 71.4 s due to the smaller number of nodes and elements. Although the conventional BEM is faster for this problem, it is restricted to homogeneous anisotropic materials. However, the BFEM introduces an interface between subregions with shared nodes and boundary elements, enabling the modeling of hybrid composite materials with distinct properties. While this approach requires a denser mesh and a longer computation time, it provides substantially greater modeling flexibility. Fig. 3 and Table 2 illustrate the hoop stress distribution around the right hole. The BFEM results show excellent agreement with those obtained by the conventional BEM, both in trend and magnitude, with discrepancies below 0.05% at selected points along the hole boundary.

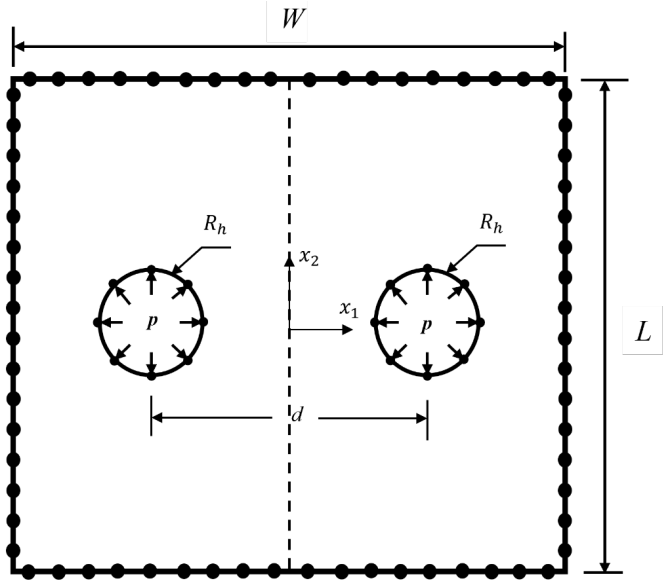

Fig. 2. Two circular holes subjected to internal pressures $p_1 = p_2 = \sigma$

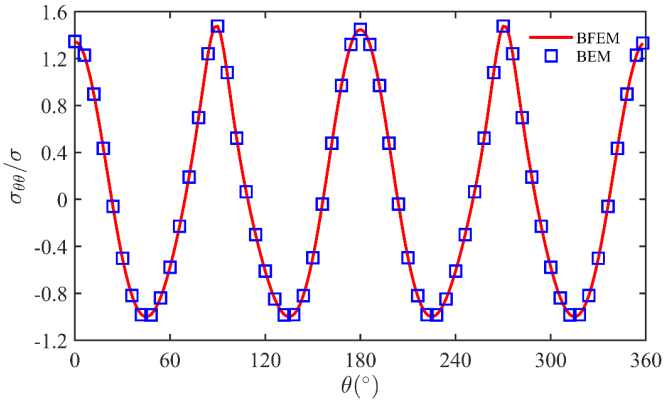

Fig. 3. Hoop stress at the right hole

3.2. Two loaded holes in an anisotropic hybrid composite plate

All of the conditions are the same as in the previous numerical example, except that each subregion is made of a different anisotropic composite material (Fig. 4). The anisotropy of the materials is expressed by the angles β_1 and β_2. The first subregion is made of material 1, which is the unidirectional fiber composite as described in Eq. (10) with $\beta_1 = 0^\circ$. The second subregion is made of material 2, which is also composed of the unidirectional fiber composite material in Eq. (10), but its fiber orientation is now rotated by the angle $\beta_2 = \beta$ from the x_1 axis.

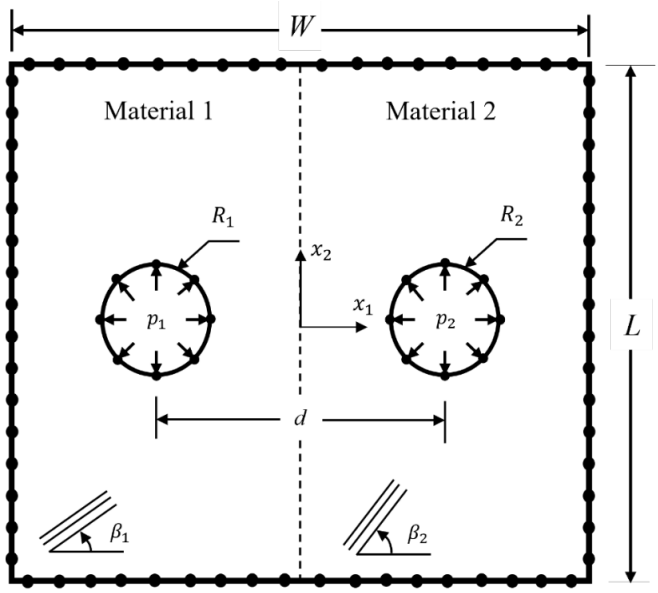

Fig. 4. An anisotropic hybrid composite plate with two circular holes loaded by the uniform internal pressure $p_1 = p_2 = \sigma = 50$ MPa

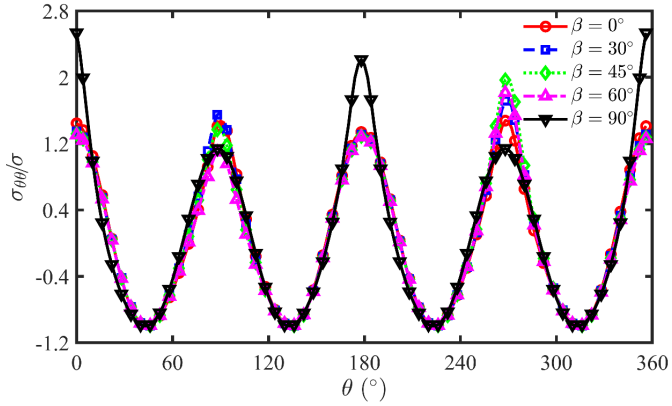

Fig. 5. Hoop stress around the left hole with different values of the fiber orientation β

Figs. 5 and 6 depict the hoop stress around the left hole for different fiber orientations of Material 2. From these figures, we can observe that the fiber orientations significantly influence the stress values on the hole. Table 3 shows that the stress distribution of the two holes is symmetric with respect to the x_2 axis when the angle is $\beta = 0^\circ$. The stress distribution around the two holes is no longer symmetric when $\beta \neq 0^\circ$. The variation of the stress is quite complex, which should be considered carefully when designing engineering applications with loaded holes in anisotropic hybrid composite plates.

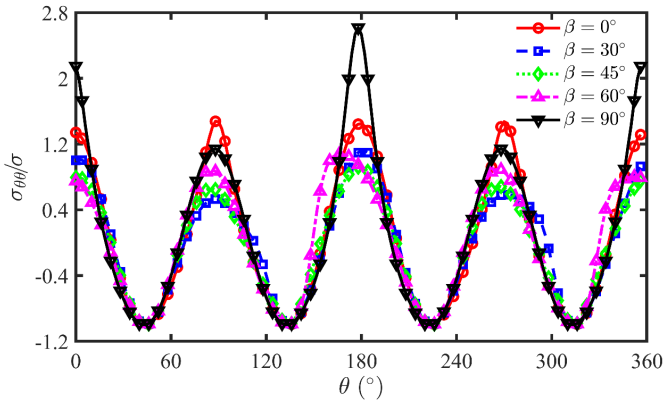

Fig. 6. Hoop stress around the right hole with different values of the fiber orientation β

Table 3. Hoop stress on the two holes with different values of the fiber orientation β

β	Hole left 90°	Hole right 90°	Hole left 0°	Hole right 180°	Hole left 270°	Hole right 270°
0°	1.4757	1.4757	1.4480	1.4480	1.4757	1.4757
30°	1.5474	0.5294	1.3482	1.0961	1.7166	0.5796
45°	1.3693	0.6467	1.3182	0.9186	1.9675	0.6828
60°	1.0976	0.8672	1.3021	0.9476	1.8140	0.8878
90°	1.0796	1.1693	1.2998	2.7104	1.1330	1.1633

3.3. Interference fits in an anisotropic hybrid composite plate

In this section, we consider an anisotropic hybrid composite plate with holes loaded by a prescribed displacement due to interference fits. The holes have dimensions $R_1 = R_2 = R =$ 5 mm and are loaded by the prescribed displacement $u_r = R_b - R$, where R_b is the radius of the bolt/rivet/pin used in the interference fit joints. The distance between the two loaded holes is denoted by $d/R = 6$ (see Fig. 7). The plate has dimensions of $W = L = 1$ m and is also made of an anisotropic hybrid composite material. The hybrid composite plate consists of two regions: one is made of the unidirectional fiber composite material as described in Eq. (10), with the fiber orientation angle equal to zero from the x_1 axis, and the other is made of the same unidirectional fiber composite material but with the fiber orientation angle being 45° from the x_1 axis. The interference fit size is defined as $\Delta = (u_r/R) \times 100$ (%). To investigate the influence of the interference fit size on the stress distribution in anisotropic hybrid composite plates, we select Δ as $\Delta = 1, 2, 3, 4$, and 5%.

Figs. 8 and 9 show the hoop stress around the holes with different interference fit sizes. It can be observed from Fig. 8 that as Δ increases, the hoop stress around the hole also increases. The distribution of the hoop stress around the left hole appears to be symmetric. At $\theta = 90°$ and $\theta = 270°$, the hoop stress rises significantly, reaching a maximum when $\Delta = 5\%$. As for the right hole, as shown in Fig. 9, the hoop stress also increases with a larger Δ, but the stress behavior shows a noticeable asymmetry since the hole is located in the material region with $\beta = 45°$, which has different material characteristics compared to $\beta = 0°$ region. This example shows the applicability of the BFEM to problems of interference fits in an anisotropic hybrid composite material, highlighting the contribution of our paper.

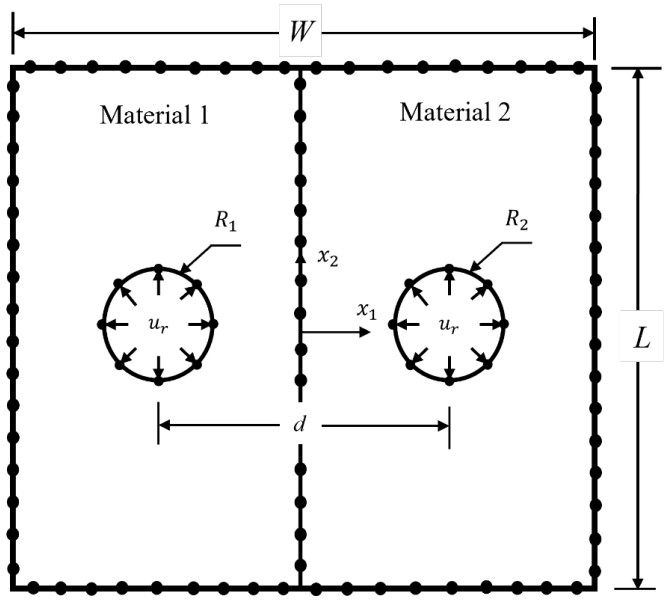

Fig. 7. An anisotropic hybrid plate with holes loaded by displacement prescribed due to the interference fit joints

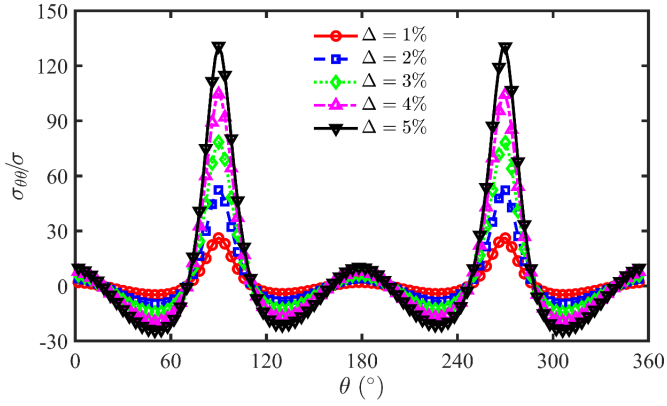

Fig. 8. Hoop stress at left hole vs. interference fit sizes

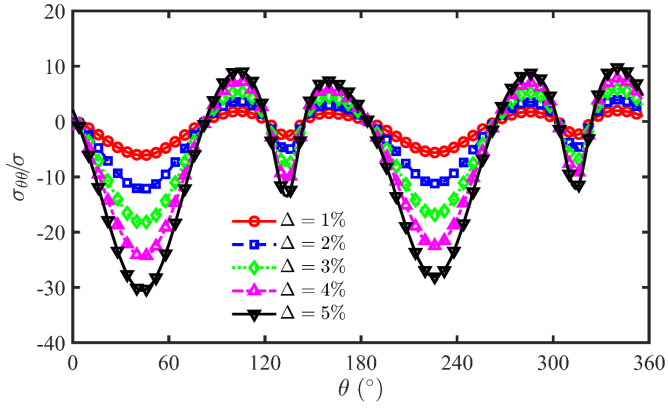

Fig. 9. Hoop stress at right hole vs. interference fit sizes

4. CONCLUSIONS

In this paper, we have successfully applied the BFEM to the stress analysis of loaded holes in anisotropic hybrid composite plates. The BFEM was validated through a comparison with the conventional BEM for a homogeneous composite plate. The results indicate that the BFEM results are well-matched with the BEM results with a deviation of less than 0.05%, which confirms the high reliability of the BFEM for the present problems. The applicability of the method is demonstrated by problems with two loaded holes in an anisotropic hybrid composite plate. In these cases, the holes are loaded either by internal pressure or by prescribed displacements due to interference fits. Through the numerical examples, parametric studies were also conducted. We revealed that the anisotropy and interference fit size have strongly influenced the stress distribution around the holes. These factors need to be considered when designing engineering applications with hybrid composite materials, and the BFEM can serve as a potential tool for this purpose.

DECLARATION OF COMPETING INTEREST

The authors declare that they have no known competing financial interests or personal relationships that could have appeared to influence the work reported in this paper.

CREDIT AUTHOR STATEMENT

Nguyen Cong Minh: *Formal analysis, Investigation, Methodology, Validation, Visualization, Writing – original draft*. Nguyen Hoang Quan: *Investigation, Supervision, Writing – review & editing*. Nguyen Van Thuong: *Conceptualization, Methodology, Resources, Supervision, Writing – review & editing*.

ACKNOWLEDGMENT

Nguyen Cong Minh was funded by the Master, PhD Scholarship Programme of Vingroup Innovation Foundation (VINIF), code VINIF.2024.ThS.07.

REFERENCES

Abazadeh, B., & Shishevan, F. A. (2019). An estimation of fatigue crack initiation and growth lives of Al 2024-T3 in double lap bolted joints with interference fitted holes. *Engineering Failure Analysis*, *105*, 1018–1031. https://doi.org/10.1016/j.engfailanal.2019.07.054

Bahloul, A., Mhalla, M. M., & Bouraoui, C. (2018). Crack repair of SENT specimen using the interference fit process. *Journal of Alloys and Compounds*, *748*, 363–374. https://doi.org/10.1016/j.jallcom.2018.03.142

Bi, Y., Jiang, J., & Ke, Y. (2015). Effect of interference fit size on local stress in single lap bolted joints. *Advances in Mechanical Engineering*, *7*(6), 168781401559030. https://doi.org/10.1177/1687814015590307

Chen, Y. C., & Hwu, C. (2014). Boundary element method for vibration analysis of two-dimensional anisotropic elastic solids containing holes, cracks or interfaces. *Engineering Analysis with Boundary Elements*, *40*, 22–35. https://doi.org/10.1016/j.enganabound.2013.11.013

Hwu, C. (2021). *Anisotropic elasticity with MATLAB*. Springer.

Hwu, C., Huang, S. T., & Li, C. C. (2017). Boundary-based finite element method for two-dimensional anisotropic elastic solids with multiple holes and cracks. *Engineering Analysis with Boundary Elements*, *79*, 13–22. https://doi.org/10.1016/j.enganabound.2017.03.003

Jamir, M. R. M., Majid, M. S. A., & Khasri, A. (2018). Natural lightweight hybrid composites for aircraft structural applications. In M. Jawaid & M. Thariq (Eds.), *Sustainable composites for aerospace applications* (pp. 155–170). Woodhead Publishing. https://doi.org/10.1016/B978-0-08-102131-6.00008-6

Li, Y., Zhang, K. F., Liu, P., & Zou, P. (2015). Interface damage behaviour during interference-fit bolt installation process for CFRP/Ti alloy joining structure. *Fatigue & Fracture of Engineering Materials & Structures*, *38*, 1359–1371. https://doi.org/10.1111/ffe.12313

Lie, S. T., Yu, G., & Zhao, Z. (2000). Analysis of mechanically fastened composite joints by boundary element methods. *Composites Part B: Engineering*, *31*(8), 693–705. https://doi.org/10.1016/S1359-8368(00)00039-1

Nguyen, H. Q., Nguyen, V. T., Nguyen, C. M., & Nguyen, T. K. H. (2025). A linear superposition method for pressurized holes/cracks in 2D anisotropic elastic solids. *International Journal of Applied Mechanics*, *17*(6), 2550043. https://doi.org/10.1142/S1758825125500437

Nguyen, V. T., & Hwu, C. (2017). Holes, cracks, or inclusions in two-dimensional linear anisotropic viscoelastic solids. *Composites Part B: Engineering*, *117*, 111–123. https://doi.org/10.1016/j.compositesb.2017.01.050

Nguyen, V. T., & Hwu, C. (2018). Multiple holes, cracks, and inclusions in anisotropic viscoelastic solids. *Mechanics of Time-Dependent Materials*, *22*, 187–205. https://doi.org/10.1007/s11043-017-9349-9

Nguyen, V. T., Nguyen, T. K. H., & Nguyen, C. M. (2025). Semi-analytical method for pin-loaded joint contact in anisotropic piezoelectric plates. *International Journal of Mechanical Sciences*, *288*, 110001. https://doi.org/10.1016/j.ijmecsci.2025.110001

Nguyen-Hoang, M., & Becker, W. (2022). Open holes in composite laminates with finite dimensions: Structural assessment by analytical methods. *Archive of Applied Mechanics*, *92*, 1101–1125. https://doi.org/10.1007/s00419-021-02095-w

Pham, T., & Weijermars, R. (2020). Solving stress tensor fields around multiple pressure-loaded fractures using a linear superposition method (LSM). *Applied Mathematical Modelling*, *88*, 418–436. https://doi.org/10.1016/j.apm.2020.06.041

Puttegowda, M., Rangappa, S. M., Jawaid, M., Shivanna, P., Basavegowda, Y., & Saba, N. (2018). Potential of natural/synthetic hybrid composites for aerospace applications. In M. Jawaid & M. Thariq (Eds.), *Sustainable composites for aerospace applications* (pp. 315–351). Woodhead Publishing. https://doi.org/10.1016/B978-0-08-102131-6.00021-9

Rust, W. (2015). *Non-linear finite element analysis in structural mechanics*. Springer.

Song, D., Li, Y., Zhang, K., Cheng, H., Liu, P., & Hu, J. (2016). Micromechanical analysis for microscopic damage initiation in fiber/epoxy composite during interference-fit pin installation. *Materials & Design*, *89*, 36–49. https://doi.org/10.1016/j.matdes.2015.09.118

Toubal, L., Karama, M., & Lorrain, B. (2005). Stress concentration in a circular hole in composite plate. *Composite Structures*, *68*(1), 31–36. https://doi.org/10.1016/j.compstruct.2004.02.016

Wang, A., Wang, Z., Zhao, M., Zhao, Y., & Chang, Z. (2023). Effects of ply thickness and interference-fit on the bearing strength of single-lap countersunk composite joints. *Thin-Walled Structures*, *189*, 110878. https://doi.org/10.1016/j.tws.2023.110878

Weijermars, R., Pham, T., & Ettehad, M. (2020). Linear superposition method (LSM) for solving stress tensor fields and displacement vector fields: Application to multiple pressure-loaded circular holes in an elastic plate with far-field stress. *Applied Mathematics and Computation*, *381*, 125234. https://doi.org/10.1016/j.amc.2020.125234

Wintermantel, E., Mayer, J., & Goehring, T. N. (2001). Composites for biomedical applications. In K. H. J. Buschow, R. W. Cahn, M. C. Flemings, B. Ilschner, E. J. Kramer, S. Mahajan, & P. Veyssière (Eds.), *Encyclopedia of materials: Science and technology* (pp. 1371–1376). Elsevier. https://doi.org/10.1016/B0-08-043152-6/00255-2

Wu, H. C., & Mu, B. (2003). On stress concentrations for isotropic/orthotropic plates and cylinders with a circular hole. *Composites Part B: Engineering*, *34*(2), 127–134. https://doi.org/10.1016/S1359-8368(02)00097-5

Xu, G., Cheng, H., Zhang, K., Liang, B., Cheng, Y., Hu, J., & Liu, C. (2020). Modeling of damage behavior of carbon fiber reinforced plastic composites interference bolting with sleeve. *Materials & Design*, *194*, 108904. https://doi.org/10.1016/j.matdes.2020.108904

Zhang, Y., & Zhou, Z. (2022). Experimental and multiscale numerical investigation on failure behavior of satin woven carbon/carbon composites subjected to pin-loading. *International Journal of Mechanical Sciences*, *219*, 107129. https://doi.org/10.1016/j.ijmecsci.2022.107129

Zuo, Y., Cao, Z., Zheng, G., & Zhang, Q. (2020). Damage behavior investigation of CFRP/Ti bolted joint during interference fit bolt dynamic installation progress. *Engineering Failure Analysis*, *111*, 104454. https://doi.org/10.1016/j.engfailanal.2020.104454